

**GT2006-90899**

**IR STRUCTURED EMISSION-BASED SPECIATION, THERMOMETRY, AND TOMOGRAPHY  
OF CO AND H<sub>2</sub>O IN HIGH-PRESSURE COMBUSTORS**

**Neil Goldstein**  
Spectral Sciences Incorporated

**Brian Gregor**  
Spectral Sciences Incorporated

**Jamine Lee**  
Spectral Sciences Incorporated

**Stephen K. Kramer**  
Pratt & Whitney

**Stuart Kozola**  
Pratt & Whitney

**Kenneth J. Semega**  
Air Force Research Laboratories

**ABSTRACT**

Passive optical probes and high-resolution emission spectroscopy are used to provide a general-purpose real-time temperature and chemical species sensing capability. Probes can be inserted in the combustor, at the turbine inlet, in the augmentor, or at the engine exit with application as an engine development diagnostic tool that provides spatially resolved measurements of the key combustion parameters: temperature, CO concentration, and H<sub>2</sub>O concentration

Multiple probes are arrayed to collect the emitted infrared radiation over different views of the hot gas path. Line-of-sight averaged concentrations and temperatures are determined by spectral analysis of the emitted radiation along each line of sight (LOS). Spatial profiles may also be determined by simultaneous analysis of overlapping lines of sight.

The collected infrared spectra contain optically thin and optically thick features that reflect the effects of emission and absorption within the combustion region. The known spectral structure of the component spectra can be used for the automated interpretation of the observed radiance spectra in terms of concentrations and temperatures along the line of sight, and in specific volume elements of overlapping lines of sight.

In this work, we present measurements of atmospheric-pressure flames and high-pressure combustors and describe the formalism for fitting the observed spectra to a basis of simulated spectra to extract estimates of concentrations and temperatures. The spectral basis is constructed using a multi-layer radiation transport model, in which each line-of-sight or measurement volume is divided into segments of uniform

concentration and temperature. The observed radiance emanating from each segment is calculated as a function of the local physical variables. The collection of observed data, which contains a highly structured emission spectrum over each line of sight, is fit to the spectral basis to extract line-of-sight averaged physical properties, or in the case of spatial reconstruction, volume-averaged properties for each of the overlap regions.

**INTRODUCTION**

Advanced measures of the state of combustion are required to meet the efficiency and affordability goals of advanced engine programs. Passive optical sensors have potential application in two areas, 1) real time control systems and 2) non-intrusive testing during engine development. In the latter application, molecular emission spectrometry could potentially provide a detailed characterization of the local state of combustion, including spatially resolved measurements of local gas temperature and the concentrations of H<sub>2</sub>O, CO and CO<sub>2</sub>. Such data would provide a complete picture of the state of combustion similar to that provided by extractive gas sampling systems.

Current techniques for quantifying combustor exit gas temperature, efficiency, and emissions involve intrusive methods such as thermocouple and extractive gas sampling probes. Both methods physically alter the local air flow conditions and are only practical during engine development. Engines operating in revenue service have little to no real time monitoring of combustor performance and global combustor operations is typically derived from the engine system

performance as a whole. Passive optical sensors could provide accurate in-situ monitoring of CO as well as a direct measure of local gas temperature. The advantages of passive optical monitoring would lead to (1) improved understanding of combustor performance spatially; (2) non intrusive measurements of combustor performance; (3) reduced test time during combustor/engine development due to increased measurement speed of the optical system; and (4) potentially enable active control of combustor exit conditions during engine operation in revenue service, maximizing engine performance and durability.

This work builds on the Structured Emission Thermometry (SET) technology which has been used for spatially resolved temperature and concentration measurements of H<sub>2</sub>O and soot based on the analysis of water emission in the Near Infrared (NIR) spectral region [Goldstein *et al.*, 2002, 2003a, 2003b]. The NIR implementation provides an important diagnostic tool that is generally applicable to well mixed, low-soot flames, such as lean pre-mixed combustors and augmentors, but is impacted by soot emission interference in staged combustors. The current work is motivated primarily by the requirement to measure CO, and therefore operates in the mid infrared (MIR) spectral region, around 5 microns where H<sub>2</sub>O, CO, and CO<sub>2</sub>, have strong molecular emission bands. This has the added benefit of reducing interference from soot emission, allowing operation in high-soot combustors.

The conceptual overview of the SET implementation, shown, in Figure 1, is the same for both the NIR and MIR implementation. Passive optical probes are arranged in the combustor to collect light over the desired field of view, which may be a single line of sight, or overlapping lines of sight used to define specific volume elements. The light is routed to a remote readout and processing module using either fiber optics (NIR implementation) or waveguides (MIR implementation). The collected emission from each lines of sight is dispersed to yield an emission spectrum. Each spectrum can be fit to provide a line-of-sight average of the observed physical properties (radiance, temperature, concentration, pressure, etc.). Alternatively, a collection of spectra corresponding to many overlapping lines of sight may be simultaneously fit using an algebraic tomographic reconstruction to determine the local spectrum in the overlap regions and the local physical properties [Goldstein 2003a].

The spatial resolution of the measurement is determined by the number of views used in the reconstruction. Real-time measurements are limited by the number of simultaneous views, which is typically of order 10. Time averaged spatial maps can be constructed using a scanning mechanism, similar to that used for gas samplers, to scan the probes across the annular gas flow, providing hundreds or thousands of views for detailed reconstruction. The current instrument, which collects data at 70 Hz, might be used to sweep across the combustion field in 5 seconds, collecting 1000 lines of sight and providing a reconstruction with a spatial resolution of a small fraction of a cm.

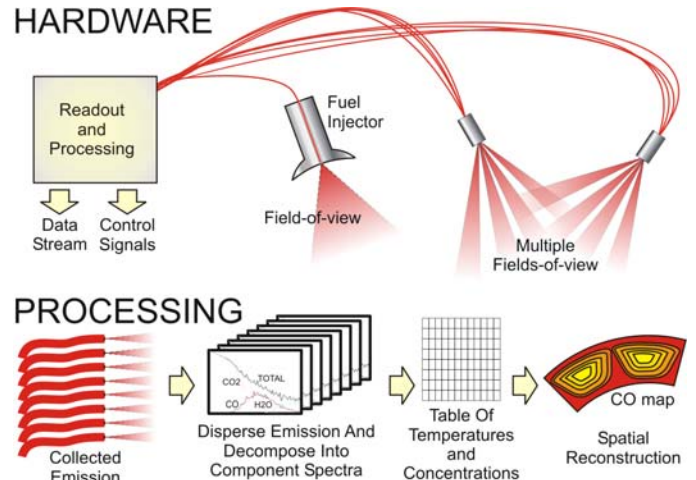


FIGURE 1. MEASUREMENT CONCEPT

The requirement to detect CO adds several challenges in both the instrumentation and the interpretation of the spectra. CO has a limited number of emission features, corresponding to the progression of vibrational overtones at 4.6, 2.3, and 1.6 microns. Each of these bands consists of a regular pattern of well-separated lines. In order to detect low levels of CO emission against a background of H<sub>2</sub>O, CO<sub>2</sub>, and soot emission, we have chosen to use high resolution, line-resolved measurement in the vicinity of 5 microns, where the CO features are interspersed among water features. We resolve the emission over a 100 nm range containing thirty CO lines and several hundred H<sub>2</sub>O lines and then uses pattern matching to fit the known spectral shapes of each molecule. As the spectral shapes are dependent on the local temperature, pressure, and density of the emitting molecules, the spectral fit can be used to determine the values of these physical properties.

We describe here preliminary laboratory-scale, and combustor test stand measurements made with a prototype instrument. The physical implementation of the MIR detection hardware is similar to, but more challenging than, the NIR instrument described previously. The principal challenges involve the implementation of hollow-core waveguides to transmit the emitted radiation, the use of a high-resolution spectrograph, and the additional cooling requirements of mid-wave array detectors.

The greatest technical challenges however are in the interpretation of the observed spectra, as the detected radiation includes both optically thin, and optically thick spectral features. This means that the observed radiation spectrum includes contributions from both emission and absorption along the line of sight, and the observed radiance is no longer a local property of the emitting volume. Fortunately, the majority of the spectral features have limited optical depth, which allows the system to see through the entire flowing gas stream.

The fitting of the spectra and the reconstruction of the local radiance require a fairly sophisticated Radiation Transport (RT) model to account for the full spectrum as observed by the probe. Future work will develop an iterative formalism for

spatial reconstruction based on this radiation transport model. In this work, we describe the RT model and its application for fitting the LOS spectra and extracting LOS averaged physical properties such as temperature and concentration ratios.

## NOMENCLATURE

$C_{ij}$	Coefficients for spectral fit
$\langle D_i \rangle$	Projected column density of species
$D_{ij}$	Column density of basis function
F	Fahrenheit
F/A	Mass Fuel air ratio
$I(\lambda)$	Observed Intensity
$\langle I_i \rangle$	Projected intensity of species
IR	Infrared
K	Kelvin
$L_{LOS}(\lambda)$	Line of Sight radiance
$L_s(\lambda, T_s, \rho_{si})$	Segment-leaving radiance
LOS	Line of Sight
MIR	Mid infrared
NIR	Near Infrared
$N(T, \lambda)$	Planck black body function
P	Pressure
$T_s$	Temperature of line segment
$T_{ij}$	Temperature of basis function
$\langle T_i \rangle$	Projected Temperature of species
$T_3$	Temperature at combustor inlet
RT	Radiation Transport
$X_{ij}(\lambda, T_{sj}, \rho_{sij}, \rho_{si'j})$	Spectral basis functions
$l$	Optical path length
nm	Nanometers
psi	Pounds per square inch
$w_{ij}$	Intensity of basis function
$k_i(\lambda, T_i)$	Component absorption coefficient
$\epsilon_s(\lambda, T_s, \rho_{si})$	Segment emissivity
$\rho_{si}$	Species number density in segment
$t_s$	Segment-leaving transmittance

## EXPERIMENTAL

Atmospheric pressure propane flames with variable fuel/air ratio were prepared using an Carlisle CC++ burner with three concentric rings of air and fuel capillary jets. This results in a partially premixed flame surrounded by a diffusion flame in air. Fuel and air flow meters were used to set the flame conditions and monitor the approximate fuel/air ratio.

High pressure spectra were obtained over a pressure range of 50-250 psi and a F/A range of 0.011-0.035 in an arc-sector test combustor at the United Technologies Research Center Jet Burner Test Stand. The test article was a derivative of Pratt & Whitney's TALON (Technology for Advanced Low NOx) combustor family for aircraft engines. The combustor was designed for low emission, low operating cost, and good reliability. A single-line-of-sight optical probe was inserted into the flow stream 13" downstream of the combustor exit with a 15-degree slant path view across the flow terminating in the inner annular combustor wall at the exit of the combustor.

A midwave IR SET instrument was assembled on a portable optical bench as shown schematically in Figure 2. It consists of one or more optical probes connected to a 1/2 meter, f/9 Czerney Turner spectrograph using Ag/I coated polycarbonate hollow waveguides (Polymicro Technologies). The water-cooled probe contains an f=25 mm CaF lens near the probe tip that couples the emitted radiation into a 2-mm diameter waveguide. The waveguide is coupled to a spectrograph a few meters away. The waveguide exit is placed at the sagittal focus of the spectrograph near the entrance slit. The light enters the spectrograph, is dispersed, and reimaged with 1:3 demagnification onto the focal plane of a Santa Barbara ImageIR-LC InSb camera.

Figure 3 shows a typical dispersed image at the focal plane of the camera. In this case, a single probe is viewing the CO-rich mantle of an extremely rich atmospheric-pressure flame. The field of view shows a series of CO lines, and weaker water lines, covering a spectral range of 4903-5013 nm. The width of each feature is dominated by the instrument resolution full width of 0.79 nm. The lower portion of Figure 3 shows the spectrum obtained by projecting the intensity of each pixel onto a calibrated wavelength scale. Also shown is a spectral fit to the data as outlined in the next section.

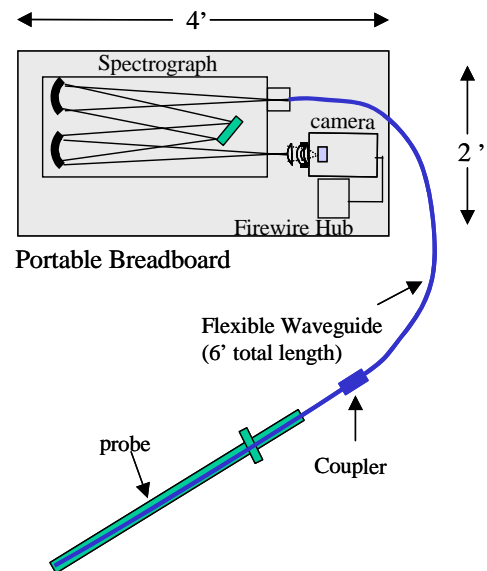
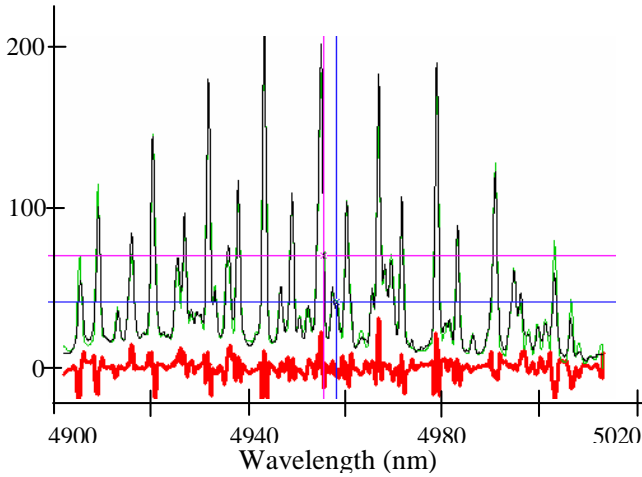
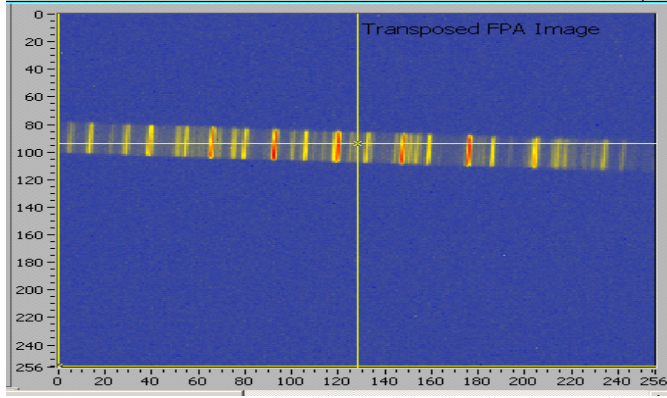


FIGURE 2. LAYOUT OF THE BREADBOARD INSTRUMENT.



**FIGURE 3. FLAME DATA. TOP: IMAGE OF A FLAME SPECTRUM ON THE FOCAL PLANE ARRAY AT THE SPECTROGRAPH EXIT. BOTTOM: PROCESSED SPECTRUM (BLACK), BEST FIT TO THE SPECTRUM (GREEN) AND RESIDUAL (RED).**

## RADIATION TRANSPORT MODEL

The interpretation of the observed spectra follows the procedures outlined previously [Goldstein *et al.* 2002, 2003]. Our approach starts with the creation of a spectral library covering all probable pressure, temperature, and concentration conditions. The observed spectra are then fit to the library and a determination of physical observables is made based on the relative contribution of each spectral library member to the fit. In this section we extend the approach to optically thick conditions.

In order to model non-uniform radiation fields, such as those seen in a combustor with non-uniform temperature and concentration, we adopt a multilayer radiation transport formalism [Berk *et al.* 1989]. In this formalism, each line of sight is broken up into a number of segments with uniform concentration and temperature. The observed radiance along the line of sight is computed based on the local radiation of each segment and the transmission of the light from the local segment, through the other segments, to the observer.

This formalism will also be essential for future spatial reconstruction efforts. The SET approach involves

reconstructing local radiance arising from each area within the field of view based on the observed radiance along multiple, overlapping lines of sight [Goldstein *et al.* 2003a]. Under optically thick conditions, the observed radiance is not a local property because of absorption in the intervening layers. Thus we must know the functional relationship between radiance and transmittance in each layer to complete the reconstruction. The multilayer approach can provide that information for each member of the spectral library.

## Multilayer Formalism

The multilayer formalism divides the line of sight into homogeneous segments characterized by a local temperature and concentration. The radiance spectrum,  $L_{LOS}$ , collected along a line of sight is represented by a sum over line segments. The contribution from each line segment is the product of the local segment-leaving radiance,  $L_s$ , and the cumulative transmittance,  $t_s$ , from the inner boundary of the line segment to the observer:

$$L_{LOS}(\lambda) = \sum_s L_s(\lambda, T_s, \rho_{si}) t_s \quad (1)$$

The local radiance is determined by the local temperature,  $T_s$ , and the density of each emitter,  $\rho_{si}$ . It is the product of the Planck blackbody function,  $N_s(T_s, \lambda)$  and the segment emissivity,  $\varepsilon_s(T_s, \lambda, \rho_{si})$ , defined as one minus the transmission through the segment:

$$L_s(\lambda, T_s, \rho_{si}) = \varepsilon_s(T_s, \lambda, \rho_{si}) N_s(T_s, \lambda) \quad (2)$$

$$\varepsilon_s(\lambda, T_s, \rho_{si}) = 1 - \prod_i e^{-k_i(\lambda, T_i) \rho_i dl}$$

Here the transmission is represented by the product of the local transmission spectra of all of the species,  $i$ , as given by the characteristic absorption coefficient,  $k_i(\lambda, T_i)$ , at temperature  $T_i$ , and the integral of the number density,  $\rho_i$ , over the segment path length,  $dl$ . The radiance spectrum therefore has a characteristic temperature-dependent spectral structure that can be distinguished in a spectrally resolved measurement.

The forward radiation transport calculation takes as input the temperatures and densities of each of the component species in each line segment. It calculates the local emissivity,  $\varepsilon_s(T_s, \lambda, \rho_{si})$ , and Planck function,  $N_s(T_s, \lambda)$ , on a fine spectral grid. These values are converted to the local radiance,  $L_s(\lambda, T_s, \rho_{si})$ , cumulative transmission,  $t_s$ , and observed radiance,  $L_s(\lambda, T_s, \rho_{si}) t_s$ , for each segment. These segment-specific variables are stored along with the line of sight radiance,  $L_{LOS}(\lambda)$ . The observed line of sight radiance is then degraded to the instrument resolution for comparison to the observed data.

## Spectral Fit

For purpose of interpreting the spectra, it is useful to fit the spectra to a set of molecule-specific basis spectra,  $\{X_{ij}(\lambda, T_{sj}, \rho_{sij}, \rho_{si'j})\}$ . For each molecular species  $i$ , a collection of  $j$  spectra are computed for all combinations of the segment temperatures, the concentration of the species of interest  $i$ , and the concentration of all other species,  $i'$ . The measured spectrum is then expressed as a linear combination of molecule-specific basis functions:

$$I(\lambda) = \sum_i \sum_j C_{ij} X_{ij}(\lambda, T_{sj}, \rho_{sij}, \rho_{si'j}) \quad (3)$$

All information about the density and temperatures of species  $i$  along the line of sight is carried by the scalar coefficients,  $C_{ij}$ . Extrinsic properties, such as radiant intensity,  $I_i$ , and column density,  $D_i = \sum_s \rho_{si}$  of species  $i$  can be determined from the weighted sum of the corresponding property for each basis function, where  $w_{ij}$  is the intensity normalization factor:

$$\langle I_i \rangle = \sum_j C_{ij} w_{ij} \quad \langle D_i \rangle = \sum_j C_{ij} D_{ij} \quad (4)$$

The line of sight weighted average of intrinsic properties, such as temperature can be determined from the ratio of weighted sums:

$$\langle T_i \rangle = \frac{\sum_j C_{ij} T_{ij}}{\sum_j C_{ij}} \quad (5)$$

In the limit of uniform temperature and composition, these weighted averages become the actual temperatures and column densities.

Concentration ratios and radiance ratios can be determined from the ratios of the component densities and intensities:

$$\frac{[i]}{[i']} = \frac{\langle D_i \rangle}{\langle D_{i'} \rangle} = \frac{\sum_j C_{ij} D_{ij}}{\sum_j C_{i'j} D_{i'j}} \quad \frac{\langle I_i \rangle}{\langle I_{i'} \rangle} = \frac{\sum_j C_{ij} w_{ij}}{\sum_j C_{i'j} w_{i'j}} \quad (6)$$

The trick in all this is to select a spectral library with sufficient elements to span all possible conditions along the line of sight. This is relatively straightforward in the optically thin limit, or in the limit of sufficiently small local segments with  $\epsilon_s \ll 1$ , where the spectra of the various component species are linearly independent.

In partially optically thick cases, the spectra can still be well described by a linear fit and useful physical information can still be extracted, as long as the spectral basis functions are reasonably characteristic of the molecular concentrations and temperatures. This often requires calculation of very large spectral libraries that contain redundant information. These large libraries can be compressed into compact molecule-specific basis containing 2-5 basis functions per molecule using Proper Orthogonal Diagonalization (POD) [Goldstein *et al.*,

2003] of each species basis. Each of the compact basis functions is then a linear combination of the larger basis set and has a characteristic value for specific physical parameters like temperature, pressure, and column density. These physical observables can be projected out to create good estimates of the local temperature, density, and concentration ratios. This process is illustrated in the following example.

## Spectral Basis for Combustor Measurements

The combustor and laboratory measurements are fit using one of four pressure-dependent spectral libraries that span the range of possible conditions at the exit of the combustor. For each pressure range (1 atm., 5-8 atm, 11-14 atm, and 17-20 atm), the library contains a total of 160 spectra for well-mixed, lean mixtures spanning a temperature range of 1000-2400K, a concentration range of  $3 < [H_2O] < 13\%$  and  $0 < [CO] < 1\%$ , a path length range of  $20 < l < 40$  cm (2-10 cm for the laboratory data). The spectra are calculated based on viewing the hot combustor through a 2 m path of cold gas between the combustor and the spectrograph.

Figure 4 shows examples of simulated spectral data for equilibrium conditions and equivalence ratios of  $0.2 < \phi < 0.6$ . Temperatures and concentrations of  $H_2O$  and  $CO_2$  are determined from the equivalence ratio using the NASA equilibrium code calculations [Mcbride and Gordon 1996]. The CO concentration is assumed to be 0.1%.

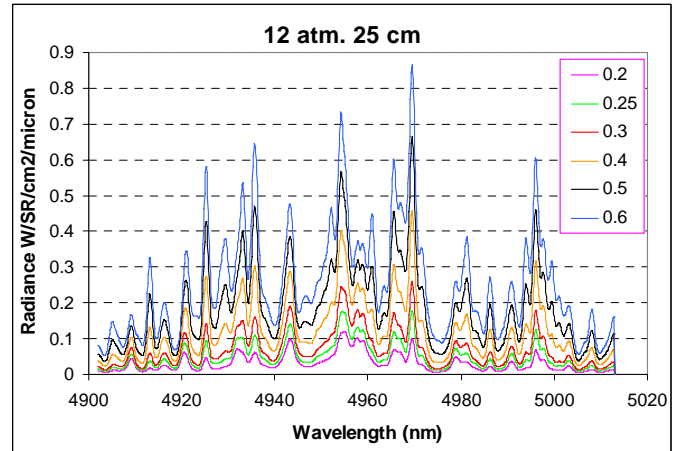


FIGURE 4. SIMULATED COMBUSTOR EXIT SPECTRA AS A FUNCTION OF EQUIVALENCE RATIO.

The CO and  $H_2O$  spectra are calculated using a line-by-line calculation based on the HITEMP spectral database [Rothman *et al.* 2000]. The  $CO_2$  spectra are based on a band model calculation [Gutowski. and Markarian 1998]. The simulated spectra are multiplied by the instrument response function, which leads to about a 50% drop off in intensity at the edges relative to the center of the spectrum.

All of the simulated spectra in Figure 4 can be fit with an accuracy of better than 99% using a compact basis of four CO basis functions and four  $H_2O$  basis functions. These basis functions were made from a singular value decomposition

(POD) of the full spectral library for each component spectrum. In constructing the spectral basis, we use the spectra of H<sub>2</sub>O, CO<sub>2</sub> and a blackbody directly. The CO spectral library is defined as the contrast spectrum with and without CO in the line of sight. This helps to linearize the problem by accounting for the absorption of CO radiation by H<sub>2</sub>O along the line of sight.

Figure 5 shows an example of a fit to the  $\phi=0.6$  simulated data. The spectrum is fit primarily with the first two water basis functions and the first CO basis function. The spectrum is predominantly due to water, but contains a 17% contribution from CO. The CO spectrum consists of two interleaved patterns corresponding to the rotational progression of two vibrational bands.

As a general rule, the first basis function of each species accounts for most of the intensity in the band, while the second basis function accounts for most of the variation with temperature. For the CO basis, the first basis function accounts for 98% of the radiant intensity at all pressures and equivalence ratios. The second accounts for most of the change in shape with temperature. The first H<sub>2</sub>O basis function accounts for 97% of the intensity and the second basis functions account for most of the temperature dependence. However, the H<sub>2</sub>O spectra contain several optically thick lines, which have a different dependence on column density than the thin lines. The contributions of these lines are described by the additional basis functions that make a large contribution to the computed column density. Thus the relative value of the H<sub>2</sub>O coefficients can be used to estimate the absolute water concentration without any knowledge of the instrument intensity calibration.

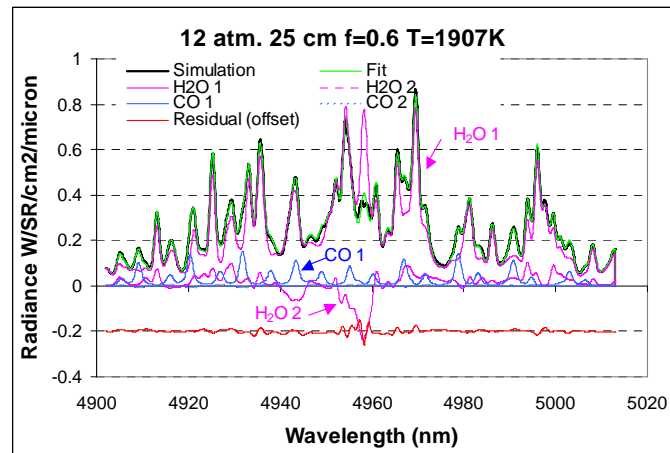


FIGURE 5. FIT TO SIMULATED SPECTRUM,  $\phi=0.6$ , SHOWING THE CONTRIBUTIONS OF THE FIRST TWO CO AND H<sub>2</sub>O BASIS SPECTRA.

### ATMOSPHERIC FLAME TESTS

A series of data were collected on atmospheric-pressure flames and fit to an atmospheric-pressure basis set composed of two basis spectra each for CO<sub>2</sub>, CO, H<sub>2</sub>O, and blackbody radiation. Figure 6 shows typical spectra obtained at the extremes of fuel air ratio: An extremely lean flame and a near-

stoichiometric flame. The fit to the H<sub>2</sub>O spectra accounts for most of the features, but there are some systematic errors, which may be related to errors or omissions in our water line list.

The two spectra have different shapes, which correspond to the different physical conditions. The shape difference is reflected in the coefficients of the spectral basis functions. In the cool, lean flame the second H<sub>2</sub>O basis function, which has a negative characteristic temperature, is added to the first. In the hot flame, it is subtracted. Only small amounts of the CO basis function are used in both fits, but the relative size of the CO coefficient is larger in the stoichiometric flame.

The differences in the spectral fit are reflected in the projected physical properties. The projected temperature values for the two spectra are  $\langle T_{H_2O} \rangle = 1525K$  for the colder flame and  $\langle T_{H_2O} \rangle = 2334 K$  for the hotter flame. The intensity values are  $\langle I_{H_2O} \rangle = 34$  counts and  $\langle I_{H_2O} \rangle = 255$  counts respectively, reflecting the higher emitter density and temperature in the near stoichiometric flame. The relative contributions of CO and H<sub>2</sub>O to the spectra are  $\langle I_{CO} \rangle / \langle I_{H_2O} \rangle = 0.022$  and  $\langle I_{CO} \rangle / \langle I_{H_2O} \rangle = 0.10$  respectively. This corresponds to concentration ratios of  $[CO]/[H_2O] = 0.0017$  and  $[CO]/[H_2O] = 0.008$ , with the higher CO concentration observed in the hotter flame.

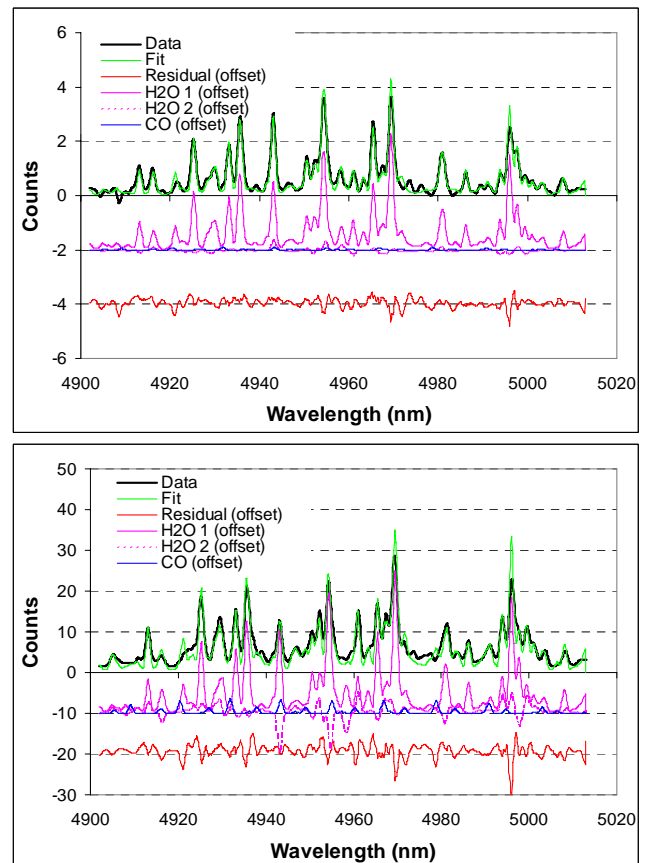
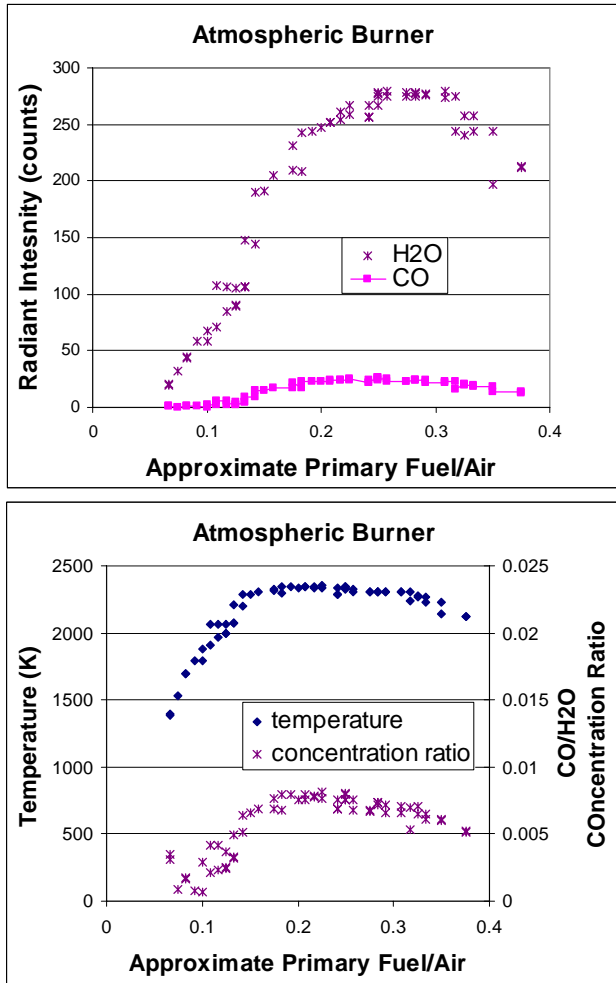


FIGURE 6. ATMOSPHERIC-PRESSURE FLAME SPECTRA. TOP: LEAN FLAME,  $T=1525K$ . BOTTOM: NEAR-STOICHIOMETRIC,  $T=2334K$ .

Figure 7 shows a compilation of the projected physical data over the full range of flame conditions. Spectral measurements were made over a fixed line of sight 4 cm above the burner while changing the fuel and airflow rates by controlling the input air and fuel flow. The flow control is not very accurate, resulting in scatter in the data, and the measured primary F/A ratio does not reflect the true F/A in the flame, as it ignores secondary mixing with atmospheric air. Yet, the overall trends illustrate that the spectrally fit properties have the anticipated functional dependence on fuel/air ratio.



**FIGURE 7. TEMPERATURE AND CONCENTRATION DATA DETERMINED FROM ATMOSPHERIC-PRESSURE FLAME SPECTRA. DATA ARE PLOTTED AS A FUNCTION OF THE MEASURED PRIMARY FUEL AIR RATIO BEFORE MIXING WITH AIR. TOP - OBSERVED RADIANT INTENSITIES OF H<sub>2</sub>O AND CO. BOTTOM - TEMPERATURES AND CONCENTRATION RATIOS.**

The fit temperature rises rapidly with increasing fuel/air and reaches a plateau of about  $2340 \pm 10$  K, which is similar to the characteristic temperature of a near stoichiometric propane/air flame. This temperature was confirmed by a second measurement using the NIR SET instrument, which also reported a temperature of  $2340 \pm 10$  K. The band-averaged

radiant intensity of H<sub>2</sub>O and CO shows a similar functional relationship. The ratio of the CO intensity to the H<sub>2</sub>O intensity yields a concentration ratio. This concentration ratio also grows with increasing F/A ratio, reaching a value of about  $0.008 \pm 0.0005$  for slightly rich flames. This corresponds to about 0.1% CO in the flame.

### COMBUSTOR TESTS

A preliminary set of combustor measurements was made to test the validity of the spectral basis functions in preparation for spatially resolved measurements to be made later. Figure 8 shows the geometry for the two tests. The ideal measurement geometry, shown in the lower drawing, would be to measure across the flow at the exit of the combustor. A traversing arm would be used to collect a series of several overlapping line-of-sight measurements for use in detailed spatial reconstruction of the flow. The current measurement geometry, shown in the upper drawing, used a convenient opening in the combustor pressure vessel to insert the probe with a line of sight (shown in blue), looking upstream at a 15-degree angle to the flow. The 35-cm long line of sight terminates at the hot combustor wall, leading to a large background blackbody signal. The gas composition is also non-uniform, as the gas has a chance to mix as it flows through the test chamber away from the combustor exit.

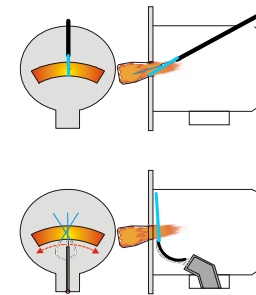


**FIGURE 8. EXPERIMENTAL GEOMETRIES.**

Spectra were obtained over a range of combustor conditions. Pressures varied from 50–250 psi. Inlet temperatures were generally between 650–900 F, except for the ignition condition data. The pressure and inlet temperature,  $T_3$ , were set at one of five predefined conditions and the fuel/air ratio was adjusted through a range of preset points. The test conditions are labeled: Ignition with Pilot Flame, Low Pressure, Mid-power I, Mid-Power II, and High-Power. Spectra were averaged for one second for each fuel/air condition.

Figures 9–11 show a selection of spectra collected in the combustor. All data were collected with a noise level of  $\sigma = 0.1$  counts/channel leading to a signal to noise ratio of  $0.1\% < S/N < 1\%$  depending on the signal strength. The figures also show spectral fits and the residual fitting error, which is always greater than the noise level. The fitting errors reflect both the truncation of the basis sets and systematic deficiencies in the spectral libraries. The former has no effect on the projected physical variables, the later can introduce systematic error. A compilation of the fit physical parameters for a larger

set of measurements is shown in Figures 12-15. All fit physical parameters have a smooth variation with F/A. The deviations from the overall trends reflect an unknown combination of errors in setting the combustor conditions and errors in the fitting process.

All of the spectra contain substantial contributions from a hot blackbody, H<sub>2</sub>O and CO. The blackbody emission comes from the hot combustor wall. The combustion gas emission rides on top of the blackbody emission. Cold water vapor absorption is also observed.

A preliminary spectral fit was conducted using the basis sets described in the previous sections. Three different basis sets are used for the gas, one for each pressure regime, 5-8 atmosphere, 11-14 atmospheres, and 17-20 atmospheres. Due to the preliminary nature of the measurements we did not bother with an exact treatment of the absorption of the wall emission by the combustion gases. Instead we treat the wall emission and gas emission as additive. Both sources experience absorption by a low-temperature regions within the probe and waveguide. The combustor is treated as a single homogeneous layer.

Figure 9 illustrates the contribution of blackbody, H<sub>2</sub>O and CO emission to the spectra. Of all the observed spectra, this spectrum has the largest relative concentration of CO. It was obtained at ignition condition with a pilot flame on. Spectra taken under similar conditions with the pilot off have a factor of two less CO contribution. The figure shows the observed spectrum, the total fit, and the contributions to the fit due to the first CO basis function and the first two water basis functions. The CO and H<sub>2</sub>O emission ride on a background of wall emission, which is not shown explicitly in the figure. Note that while H<sub>2</sub>O and CO have many overlapping lines, both molecules have well-resolved identifying features that are readily observable by eye.

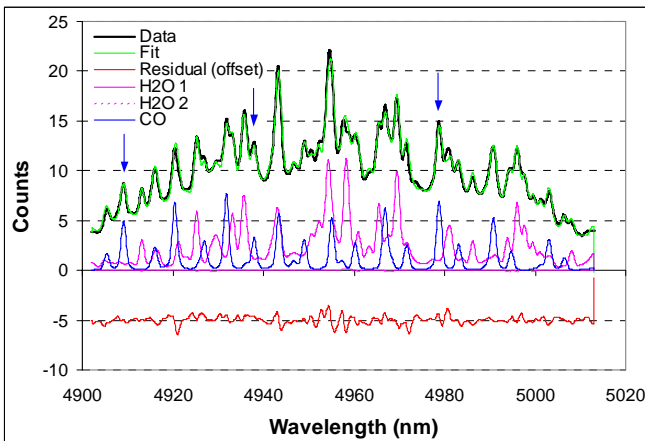


**FIGURE 9. COMBUSTOR SPECTRA WITH LARGEST CO CONTRIBUTION, IDLE WITH PILOT FLAME. BLUE ARROWS MARK WELL RESOLVED CO FEATURES.**

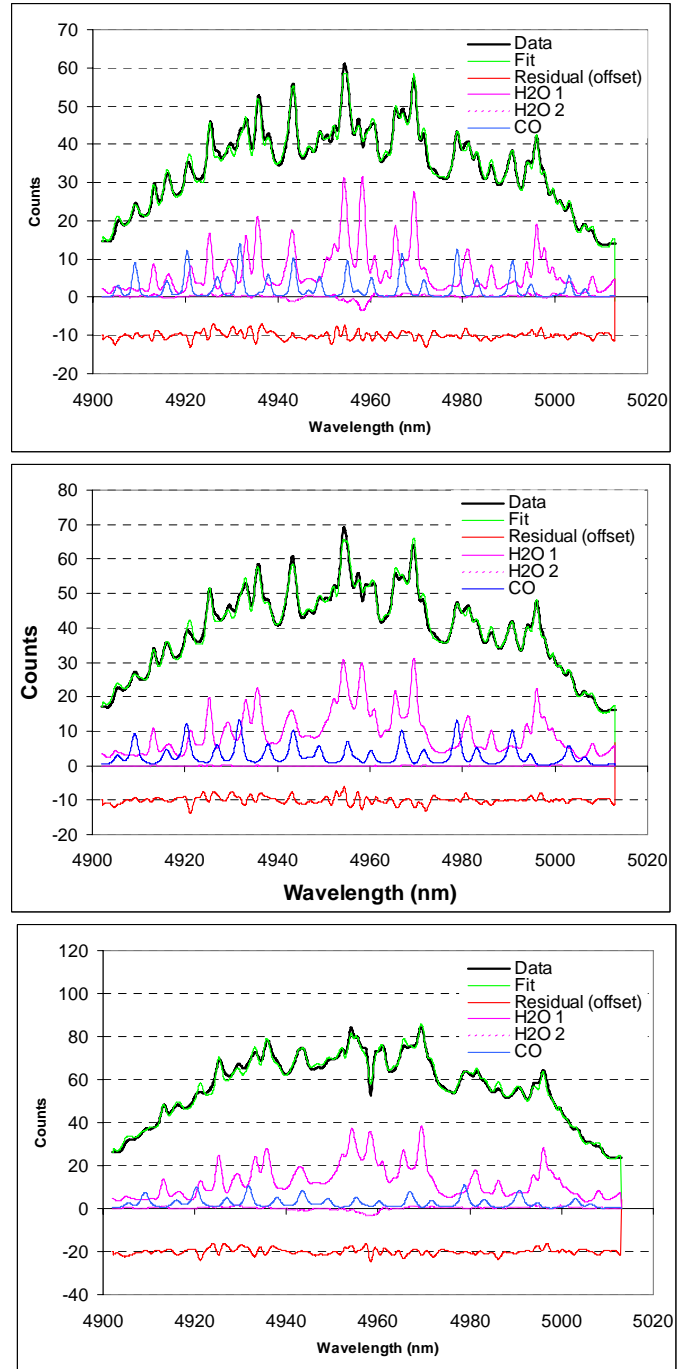
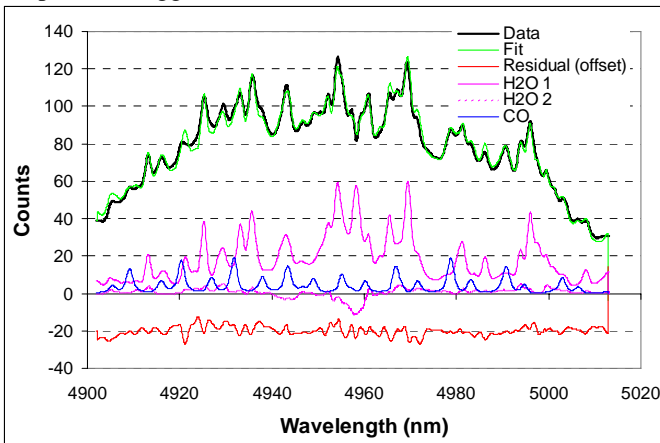


**FIGURE 10 SPECTRAL VARIATION WITH PRESSURE, F/A=0.022. TOP: LOW PRESSURE, MIDDLE: MID-POWER II, BOTTOM: FULL-POWER.**

Figure 10 illustrates the effect of pressure on the observed spectra. It compares three spectra taken at F/A=0.022 but with different pressures. The CO and H<sub>2</sub>O features become wider with increasing pressure, reflecting the pressure broadening in the combustor. The spectral fits adequately reflect this variation with pressure and retrieve appropriate physical observables. For example the fit temperatures for the three

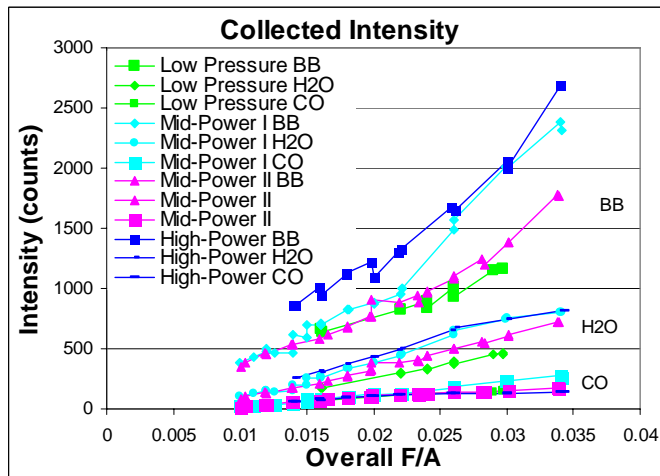
different pressure conditions are  $\langle T_{H_2O} \rangle = 1718K, 1662K,$  and  $1715K$  respectively. These temperatures are higher than the equilibrium temperature for fully mixed exhaust, and are characteristic of a local fuel/air ratio of about  $F/A=0.032$ .

Figure 11 shows a higher temperature spectrum obtained under Mid-power II conditions and  $F/A=0.034$ . This should be compared to the middle spectrum in Figure 10. The water features in the spectrum are qualitatively different and result in a projected water temperature of  $T_{H_2O}=1950K$ . This temperature suggests a local fuel/air ratio of about  $F/A=0.04$ .



**FIGURE 11. HIGH F/A SPECTRA –MID-PRESSURE II,  $F/A=0.034$**

The results of the fit to all of the data are summarized in Figures 12-15. Figure 12 shows the relative radiance of the blackbody,  $H_2O$  and  $CO$  as a function of fuel/air ratio. All three signals increase with increasing pressure and fuel/air ratio. The wall radiation accounts for about 70% of the radiation, the water accounts for about 25% of the radiation, and the  $CO$  for about 5% of the radiation



**FIGURE 12. INTENSITY OF THE BLACKBODY,  $H_2O$  AND  $CO$  RADIATION AS A FUNCTION OF COMBUSTOR CONDITION.**

Figure 13 shows the variation of the projected water temperature as a function of fuel/air ratio for each of the pressure conditions. The projected gas temperature is a smooth

function of the fuel/air ratio. The gas temperature is similar for all conditions, but reflects the input  $T_3$  and pressure conditions. Figure 13 also shows the equilibrium values for two cases that bracket the data:  $P=20$  atm. and  $T_3=700K$ , and  $P=10$  atm,  $T_3=590K$ . The observed data match the equilibrium data but are shifted along either the temperature or  $F/A$  axis. This most likely reflects uneven mixing in the exhaust, but may also include a systematic error in our spectral models.

Figure 14 shows the variation in the relative intensity of  $\langle I_{CO} \rangle / \langle I_{H_2O} \rangle$ . The relative contribution is fairly constant, but varies smoothly with  $F/A$  with a peak at about  $F/A=0.02$ . The  $CO$  contribution is substantially larger than that observed in the atmospheric-pressure burner. It is largest for the low-pressure condition, and smallest for the high-pressure High Power condition.

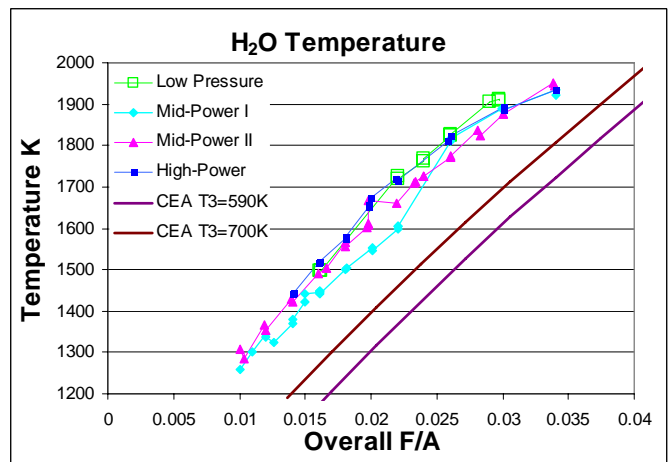


**FIGURE 13. PROJECTED  $H_2O$  GAS TEMPERATURE AND EQUILIBRIUM TEMPERATURE VALUES.**

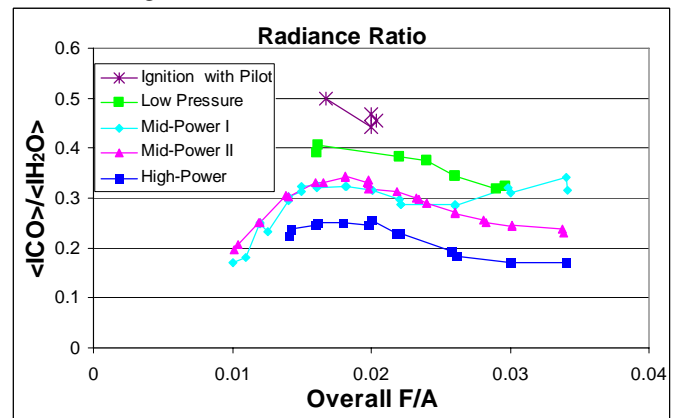


**FIGURE 14. INTENSITY RATIO  $\langle I_{CO} \rangle / \langle I_{H_2O} \rangle$ .**

Figure 15 shows an estimate of the local concentration of  $CO$  based on the assumption of a homogeneous gas mixture and homogeneous temperature within the line of sight, and equilibrium water concentration. This is a very rough estimate, as the assumption of a homogeneous field is a poor one for this geometry.

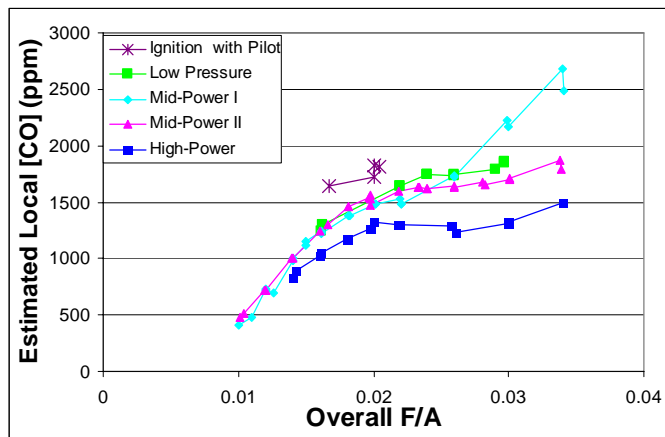


FIGURE 15. ESTIMATED LOCAL CO CONCENTRATIONS.

This estimate can be compared to concentrations obtained by gas sampling probes at the combustor exit. There is a reasonable correlation between the two sets of data, but the estimate based on the optical measurement is typically a factor of five to ten times higher than the gas sample data. While our estimate is preliminary and only semi-quantitative, it is clear from the spectra that there is an appreciable amount of CO along the line of sight that is not detected with the extractive gas sampler. This reflects in part the effects of inhomogeneity within the combustor. [CO] is a non-linear indicator of mixing and therefore small areas of locally rich exhaust gas near the walls or in embedded in the gas stream can lead to large differences in the line-integrated CO concentration. This is precisely the reason why localized, in-situ measurements of CO concentration are needed for combustor testing.

In summary, both the optical temperature results and the CO concentration results have a consistent and reproducible relationship to the combustor operating conditions, which can be measured over a wide range of pressures. The measured temperature and CO concentrations are both consistently higher than that predicted for a well mixed exhaust at equilibrium. Most likely this reflects the local values in the rich regions of a partially mixed exhaust stream.

## DISCUSSION AND CONCLUSIONS

We have demonstrated Structured Emission Thermometry and concentration measurements over a large range of pressures, temperatures and optical depths using line-resolved mid-infrared instrumentation. The observed 5-micron spectra of CO and H<sub>2</sub>O can be adequately described by existing theoretical spectral databases and the experimental spectra can be fit to the theoretical spectral libraries to extract physical information about the gases in the line of sight. We have demonstrated experimentally the extraction of temperatures and species concentration ratios. Our simulations suggest that other physical properties, such as absolute species concentration and pressure may also be extracted using the proper combination of viewing geometry and spectral range.

We have implemented and demonstrated a multilayer formalism for constructing the spectral libraries that explicitly accounts for local variations in temperature and species densities along the line of sight. This multilayer formalism will be required in future efforts aimed at spatially resolved measurements of the local spectral and physical properties. In future work, we will obtain data from multiple overlapping views and fit it to local radiance in order to determine spatially resolved maps of the physical properties.

Future application of this technology can be tailored to measure specific physical parameters of interest. This may involve changes in the spectral range and resolution of the measurement hardware and viewing geometry to take advantage of the information content inherent in the spectra of the gas stream.

We are currently pursuing one such application, which is the development of robust test instrumentation for high spatial-resolution measurements of [CO], [H<sub>2</sub>O], and temperature pattern factors at the exit of the combustor. Using a rotating sampling arm and hardware similar to that used in these breadboard measurements, we should be able to make spatially resolved measurements at a standoff distance of 10 m. These measurements may be made relatively rapidly, on a time scale of ten seconds, and with a spatial resolution better than 1 cm.

## ACKNOWLEDGMENTS

The authors would like to thank Scott Kearney and the staff at the United Technologies Research Center Jet Burner Test Stand for their dedicated support and interest in this work. This work was sponsored by the U.S. Air Force Research Laboratory under Contract No. FA8650-04-C-2491.

## REFERENCES

- Berk, A., L.S. Bernstein and D.C. Robertson, "MODTRAN: a moderate resolution model for LOWTRAN7," GL-TR-89-0122, Air Force Geophys. Lab., Hansom AFB, MA, 38 pp. (1989).
- Goldstein, N., C.A. Arana, F. Bien, J. Lee, J. Gruninger, T. Anderson, W.M. Glasheen, "Innovative Minimally Intrusive Sensor Technology Development for Versatile Affordable Advanced Turbine Engine Combustors," Proceedings of the ASME Turbo Expo, 2002, GT-2—2300051(2002).
- Goldstein, N., S.M. Adler-Golden, X. Jin, S.C. Richtsmeier, J. Lee, and C.A. Arana, "Temperature and Temperature Profile Measurements in the Combustor Flowpath using Structured Emission Thermography," Proceedings of the ASME Turbo Expo, 2003,GT2003-38695 (2003a).
- Goldstein, N., J. H. Gruninger, F. Bien, J. Lee, "System and Method for Optically Determining Properties of Hot Fluids from the Spectral Structure of Emitted Radiation," Patent US6640199 (2003b).
- Gutowski, R.M. and P. Markarian, "Standard Plume Ultraviolet Radiation Code (SPURC): Low Altitude (LA) 1.3 Users Manual," PL-TR-97-3018 (September 1998).
- McBride, B. J. and S. Gordon, "Compute Program for Calculation of Complex Chemical Equilibrium Compositions and Applications," NASA Ref. Pub 1311 (1996).
- Rothman, L. S. C. Camy-Peyret, J.-M. Flaud, R. R. Gamache, A. Goldman, D. Goorvitch, R. L. Hawkins, J. Schroeder, J. E. A. Selby and R. B. Wattson, "HITEMP, the High-Temperature Molecular Spectroscopic Database," (2000), available through <http://www.hitran.com>.